

Fe₃O₄ NANOPARTICLES COATED WITH Zn(II)-CARBOXYLATO COMPLEXES

M. D. ȘERB, E. VASILE, A. RĂZVAN, F. DUMITRU*, C. ANDRONESCU, O. OPREA, O. R. VASILE, A. M. HOLBAN, E. ANDRONESCU
Politehnica University of Bucharest, 1 Polizu st., 011061, Bucharest, Romania

The present paper reports on a facile and nontoxic solvothermal method for the preparation of magnetite (Fe₃O₄) coated with Zn(II)-carboxylato complexes. The magnetite nanoparticles with a narrow size distribution (average particle size 3 nm) have been directly obtained by thermal decomposition of Fe(III)-acetylacetonate in polyethylene glycol (PEG 200), which acts both as *green* solvent and as reducing agent. The nanoparticles of Fe₃O₄ have been easily dispersed in polar solvents due to their *in-situ* coating with the hydrophilic layer of polyol ligands. The as-obtained nanoparticles can be further tuned by interacting with Zn(II) - carboxylato complexes: [Zn(HC₄O₄)₂(OH₂)₄], Zn-1 and [Zn(C₉H₇O₄)₂(OH₂)₃].2H₂O, Zn-2 with the aim of obtaining functional magnetic materials, Fe₃O₄@Zn-1 and Fe₃O₄@Zn-2, with potential applications as biomaterials. Preliminary biological assays on these nanoparticles proved that Fe₃O₄@Zn-1 nanoparticles exhibit good biocompatibility in HCT-8 and MSC cell lines; flow cytometry analysis and cloning studies showed that no significant changes occurred on cell cycles upon treatment (24 h, at 37 °C and 5% CO₂) with synthesized Fe₃O₄@Zn-1 powders. High-resolution TEM (HRTEM), energy dispersive X-ray (EDX), X-ray photoelectron spectroscopy (XPS), thermogravimetry (TG) and differential scanning calorimetry (DSC) have been performed for nanoparticles characterization.

(Received March 14, 2016; Accepted May 6, 2016)

Keywords: Magnetite nanoparticles, Zn-carboxylato-complexes, Hybrid particles, Green solvent, Biocompatibility

1. Introduction

Iron-containing nanoparticles (Fe₃O₄ or γ -Fe₂O₃) and their dispersions in various solvents have been extensively studied due to their versatility and interesting magnetic, catalytic, electronic properties and biocompatibility, that confer them a great potential to be used in high-technology applications as: solar cells [1], heterogeneous catalysis [2, 3], biological labelling, detection and magnetic separation, target-drug delivery, hyperthermia therapy, tissue engineering [4] and magnetic resonance imaging (MRI) [5-15].

For most of these applications, the iron-containing magnetic nanoparticles are required to be water-soluble, monodisperse, superparamagnetic and easily to be produced in multigram scale [16].

There are several methods described as efficient in the preparation of water-soluble Fe₃O₄ nanoparticles: coprecipitation, sol-gel, microemulsion, hydrothermal/solvothermal, sonochemical and flame spray pyrolysis processes [17-20]. In order to overcome the agglomeration and precipitation tendency of Fe₃O₄ nanoparticles in water, various coatings that bring them stability have been studied [8, 16].

Thus, electrostatic, hydrophobic, chelating and covalent interactions have been employed to stabilize the surface of iron oxides (Fe₃O₄ or γ -Fe₂O₃) nanoparticles with the prerequisite of the presence of hydroxyl groups (Fe-OH), on nanoparticle surface [16]. The stability of these nanoparticles has been improved in terms of chemical and thermal resistance by covering them

*Corresponding author: d_florina@yahoo.com

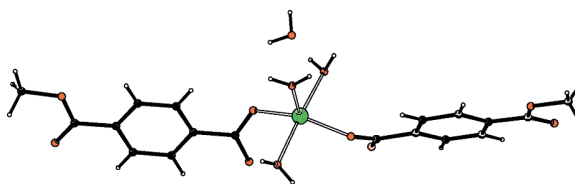
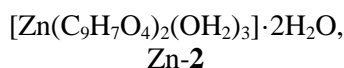
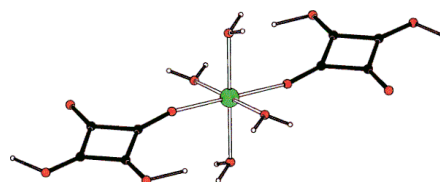
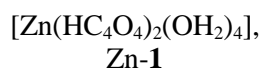
with silane [21], carboxylic acids [16], phosphonic acid [22], dopamine [23], polymers (dextran, poly(ethylene oxide), poly(vinyl alcohol), poly(vinylpyrrolidone), poly(imine), poly(acrylic acid)) [16].

The polyol process - a solvothermal method based on the partial reduction of Fe(III) to Fe(II) with di-, tri-, polyethylene glycols (PEGs of different molar weights) - proved to be one of the most efficient route for synthesis of Fe₃O₄ nanoparticles. In this polyol process PEGs act as solvents, reducing agents and also as stabilizers, in order to prevent particles agglomeration [8, 16, 24-27]. Moreover PEGs are environmentally friendly, amphiphilic and biocompatible reagents, thus, the method represents a *green* synthetic approach in preparing Fe₃O₄ nanoparticles [28, 29].

In the case of biomagnetic applications, the presence of a polymer coating could bring colloidal stability (steric stabilization) and also surface functionality, thus giving the possibility of designing hybrid particles (*e.g.* the Fe₃O₄ nanoparticles properties can be further tuned by incorporating of other biological metals into the structure) [18].

We report the preparation and characterization of water-soluble Fe₃O₄ nanoparticles coated with Zn(II)-carboxylato complexes (carboxylate moieties originate from either monosquarate anion, HC₄O₄⁻ or mono methylterephthalate, C₉H₇O₄⁻) designed for potential biomedical applications.

Fe₃O₄ nanoparticles with hydroxyl groups (Fe···OH) on the surface (average particle sizes of 3 nm), have been obtained by thermal decomposition of Fe(acac)₃ (acac – acetylacetonate) in a high-boiling solvent PEG 200 (molar weight). The Fe₃O₄ nanoparticles coated with a PEG layer are chemically active and available for further functionalization. The aqueous dispersion of these nanoparticles has been reacted with Zn(II)-complexes [Zn(HC₄O₄)₂(OH₂)₄], Zn-1 [30] and respectively [Zn(C₉H₇O₄)₂(OH₂)₃].2H₂O, Zn-2 [31] (Scheme 1), yielding Fe₃O₄@Zn-carboxylates (Fe₃O₄@Zn-1, Fe₃O₄@Zn-2) coated nanoparticles.



Scheme 1. Crystal structure representation of Zn(II)-carboxylato complexes Zn-1, Zn-2
Zn-green, O-red, C-black [30, 31].

XPS measurements, TG/DSC analyses, and HRTEM/EDX techniques were employed to characterize the morphology, size, and size distribution of the prepared materials.

In order to assess their role in biomagnetic applications, biological assays on the Fe₃O₄@Zn-1 and Fe₃O₄@Zn-2 are underway.

2. Experimental

2.1. Techniques and materials

All the chemicals were commercially available and used as received.

Thermal analyses TG-DSC of the compounds were carried out with a Netzsch 449C STA Jupiter. Samples were placed in open Pt crucible and heated with 10 degrees·min⁻¹ from room temperature to 900 °C under the flow of 20 mL·min⁻¹ dried air. An empty Pt crucible was used as reference.

TEM and HRTEM images were taken using a TECNAI F30 G² high-resolution transmission electron microscope operated at an accelerating voltage of 300-kV device. The samples have been prepared by dispersing a large number of product particles by ultrasonication in methanol and subsequently collected into a holey carbon-coated TEM support grid.

X-ray photoelectron spectroscopy (XPS) data were recorded on a Thermo Scientific K-Alpha equipment, fully integrated, with an aluminium anode monochromatic source (1486.6 eV). The survey spectra were registered using a pass energy of 200 eV at bass pressure of 2×10⁻⁹ mbar.

2.2. Synthesis of Zn(II) carboxylato-complexes

[Zn(HC₄O₄)₂(OH₂)₄], Zn-1 and [Zn(C₉H₇O₄)₂(OH₂)₃]·2H₂O, Zn-2

The colorless crystals of Zn-1 and Zn-2 have been obtained by slow evaporation in air of aqueous mixture of Zn(NO₃)₂·6H₂O (1eq) with H₂C₄O₄ (1eq), for Zn-1 and respectively with C₉H₇O₄Na (1eq), for Zn-2, as described previously [30, 31].

2.3. Preparation of Fe₃O₄@PEG and Fe₃O₄@Zn-carboxylates nanoparticles

Fe₃O₄@PEG magnetic nanoparticles were synthesized without any additional stabilizer and dispersant according to the following procedure.

Red crystals of Fe(acac)₃ have been prepared from FeCl₃·6H₂O, NH_{3(aq)} and acetylacetone in excess (yields~90%).

20 mmol of Fe(acac)₃ dissolved in 20 mL PEG 200 were stirred and heated at 280 °C for 2 h. The color of the solution turns from red to black. After cooling at room temperature, a black suspension is formed. The precipitated powder of Fe₃O₄@PEG could be magnetically separated from the reaction mixture, washed for several times with deionized water and ethanol.

Fe₃O₄@Zn-carboxylates nanoparticles (Fe₃O₄@Zn-1 and Fe₃O₄@Zn-2)

47 mg of as-synthesized Fe₃O₄@PEG and 120 mg Zn-1 have been sonicated in 10 mL deionized water, for 20 min.

67 mg of as-synthesized Fe₃O₄@PEG and 100 mg Zn-2 have been sonicated in 10 mL deionized water, for 20 min.

The resulting products Fe₃O₄@Zn-1 (Fe₃O₄@PEG coated with Zn-1) and Fe₃O₄@Zn-2 (Fe₃O₄@PEG coated with Zn-2) have been separated from the solution using a neodymium magnet, and washed with ethanol.

2.4. Flow cytometry analysis and cloning studies

Each sample was weighed to obtain 100 mg/mL stock concentration. HCT cells were cultured for 24 h in 3.5 cm diameter Petri dish by seeding 3.5 × 10⁵ cells in each well. Cultured cells were treated with 1 mg/mL compound (final concentration). After 24 hours, cells were harvested, washed in phosphate buffer saline (PBS, pH = 7.5), fixed in 70% cold ethanol and maintained overnight at -20 °C. Each sample was washed in PBS, treated with 100 µg/mL RNase A for 15 min and colored with 10 µg/mL propidium iodide by incubation at 37 °C, for 1 h.

The data acquisition was made by using Epics Beckman Coulter flowcytometer, analyzed with FlowJo software and expressed as fractions of cells in different cycle phases.

Cloning studies

HCT cells have been used for the cytotoxicity assay. The cells have been cultured in RPMI 1640 media (Sigma-Aldrich, USA), containing 10% fetal calf serum (FCS) and penicillin/streptomycin (100 U/mL). Cell cultures have been incubated at 37 °C, and 5% CO₂.

Approximately 10⁵ HCT cells were treated with 100 µg/mL of each compound, and seeded in 24 well plates. The compound was removed after 24 h, and the culture medium has been changed every 2 days, for up to 10 days. The cell viability was monitored periodically by using phase contrast microscopy. After 10 days, the evolution of cellular clones has been evaluated by counting the colonies after fixation with methanol and stained with crystal violet.

3. Results and discussion

3.1. Synthesis of Fe₃O₄@Zn-1, Fe₃O₄@Zn-2 nanoparticles

A *green chemistry* route was applied for the preparation of Fe₃O₄@Zn-carboxylates nanoparticles as follows: water-soluble magnetite nanoparticles Fe₃O₄@PEG have been synthesized by thermal decomposition of Fe(acac)₃ in PEG 200; the as-synthesized Fe₃O₄@PEG nanoparticles, having hydroxyl groups on their surface, have been coated with Zn(II)-complexes, Zn-1 and Zn-2.

In this polyol process, PEG 200 acts as high-boiling solvent, reducing agent for Fe(III) to Fe(II), and also as stabilizer, in order to prevent the particles aggregation.

Both Fe₃O₄@PEG and Fe₃O₄@Zn-carboxylates nanoparticles have potentially biomedical applications, due to the PEG-ylated magnetite nanoparticles which are effective in protein binding preventing, when used as nanocarriers and MRI contrast agents with long blood circulation times [8,16,32]. Also Zn-coordination complexes supported on magnetite nanoparticles could be applied for the extraction and release of biological compounds from aqueous media [28, 33].

3.2. Characterization of coated Fe₃O₄ nanoparticles

XPS measurements, TG/DSC analyses, and HRTEM/EDAX techniques were carried out to characterize the morphology, size, and size distribution of the prepared materials.

The results of the investigations with XPS, TEM/HRTEM/EDAX, and selected area electron diffraction (SAED) indicated that by applying the proposed synthesis route, the inverse spinel structure pure phase polycrystalline of Fe₃O₄ has been obtained.

3.2.1. XPS data

The final product in the magnetite nanoparticles synthesis, generally consists of a mixture of Fe₃O₄ and γ -Fe₂O₃ implying difficulty in differentiating them, since both phases are of the same spinel structure. XPS is one of the most effective ways to distinguish between the two phases, being also very sensitive to Fe(II) and Fe(III) cations [34].

XPS scans (Fig. 1) performed on: Fe₃O₄@PEG (a), Fe₃O₄@Zn-1 (b), Fe₃O₄@Zn-2 (c) reveal the constitutive elements: C – C1s, O – O1s, Fe – Fe2p and also Zn – Zn2p for (b) and (c), with the binding energy values collected in Table 1.

Table 1. XPS binding energies for Fe₃O₄@PEG (a), Fe₃O₄@Zn-1 (b), Fe₃O₄@Zn-2 (c)

Element	Binding energy values (eV)			
	Fe ₃ O ₄ @PEG (a)	Fe ₃ O ₄ @Zn-1 (b)	Fe ₃ O ₄ @Zn-2(c)	
C – C1s	286.44	288.08	286.08	
O – O1s	532.06	533.35	532.38	
Fe – Fe2p	Fe3p _{3/2}	57.12	58.66	57.17
	Fe2p _{3/2}	712.75	713.15	712.06
	Fe2p _{1/2}	726.26	727.29	725.40
Zn – Zn2p	Zn2p _{3/2}	–	1023.47	1022.79
	Zn2p _{1/2}	–	1046.47	1046.29
	Zn _{LMM}	–	478.33 500.91	477.08 500.32

The levels of Fe3p_{3/2}, Fe2p_{3/2} and Fe2p_{1/2} (Table 1) of 57.12–58.66 eV, 712.06–713.15 eV and 725.40–727.29 eV, respectively, are indicative for the magnetite pure phase (Fe₃O₄, Fe-O bond) [34]; whereas the levels of Fe2p_{3/2} and Fe2p_{1/2} are 710.4 and, respectively, 724.0 eV for γ -Fe₂O₃ [35].

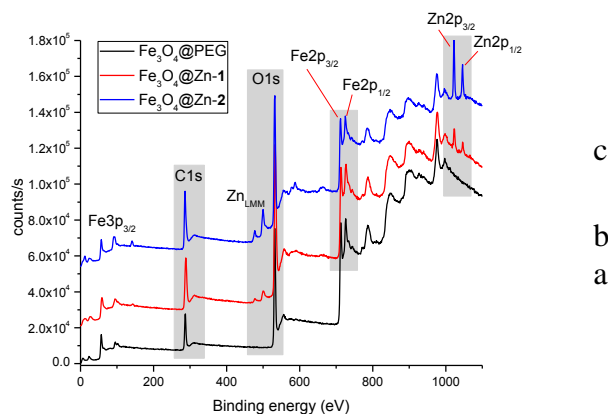


Fig.1. XPS spectra of $Fe_3O_4@PEG$ (a), $Fe_3O_4@Zn-1$ (b), $Fe_3O_4@Zn-2$ (c); the spectra for $Fe_3O_4@Zn-1$ (b), $Fe_3O_4@Zn-2$ (c) were shifted by 11000 and 36000 y-units, respectively

The C1s peaks at 286.08–288.08 eV are due to C-O-C and O-C=O bonds, arising from the adsorbed PEG 200 molecules and carboxylato-complexes to the particle surface [29].

The XPS spectra of $Fe_3O_4@Zn-1$ (b), $Fe_3O_4@Zn-2$ (c) exhibit a doublet in the Zn2p region, which could be identified as Zn2p_{3/2} lines (1022.79–1023.47 eV) and respectively as Zn2p_{1/2} (1046.29–1046.47 eV). In the range of 470–500 eV appear the Auger Zn_{LMM} lines, typical for Zn-O bonds (Table 1) [36].

The XPS results proved that PEG 200 and, subsequently, the Zn-complexes: Zn-1 and Zn-2 have been immobilized upon the Fe_3O_4 surface.

3.2.2. Thermal analysis

The presence of polyol ligands ($Fe_3O_4@PEG$) and the Zn-carboxylato complexes ($Fe_3O_4@Zn-1$, $Fe_3O_4@Zn-2$) on the surface of the magnetite nanoparticles is further supported by TG-DSC measurements.

TG-DSC curves of the $Fe_3O_4@PEG$ nanoparticles (Fig. 2) show a slight mass loss of 1.77% in the temperature range of 30–120 °C attributed to the desorption of water/solvent molecules adsorbed onto $Fe_3O_4@PEG$ nanoparticles surface. In the temperature range of 120–400 °C, the significant mass loss (25.97%) accompanied by a strong exothermic effect ($t=263$ °C) was attributed to the desorption and subsequent combustion of PEG molecules. As the combustion of PEG takes place, a transformation of Fe_3O_4 to $\gamma-Fe_2O_3$ occurred. This conversion is followed by the phase change $\gamma-Fe_2O_3 \rightarrow \alpha-Fe_2O_3$ ($t=448.6$ °C, exothermic effect without any mass loss) as the DSC curve revealed. The total mass loss (was 28.68 %) indicates that 71.32% percentage represents the iron oxide in the poly(ethylene glycol)-coated nanoparticles.

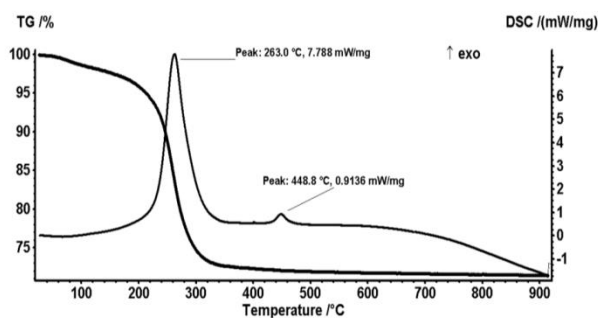


Fig. 2. TG-DSC curves of $Fe_3O_4@PEG$ over the temperature range (25–900 °C)

TG-DSC curves of the $\text{Fe}_3\text{O}_4@\text{Zn-1}$ and $\text{Fe}_3\text{O}_4@\text{Zn-2}$ nanoparticles presented in Fig. 3 and, respectively Fig. 4, indicate total mass losses of 35.88% in the case of $\text{Fe}_3\text{O}_4@\text{Zn-1}$ and 29.04% for $\text{Fe}_3\text{O}_4@\text{Zn-2}$ nanoparticles, which are comparative to the content of PEG found for the starting $\text{Fe}_3\text{O}_4@\text{PEG}$ (28.68%). Similar decomposition patterns, with minor mass losses associated to complete dehydration of the samples below 120 °C, followed by decomposition steps (combustion of PEG 200 and organic carboxylates) in the 120-400 °C temperature range, could be observed for $\text{Fe}_3\text{O}_4@\text{Zn-1}$ and $\text{Fe}_3\text{O}_4@\text{Zn-2}$ nanoparticles.

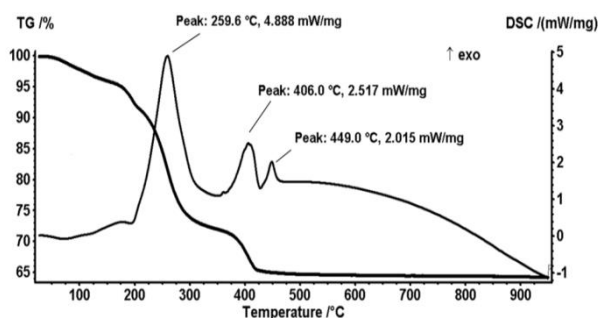


Fig. 3. TG-DSC analysis of $\text{Fe}_3\text{O}_4@\text{Zn-1}$

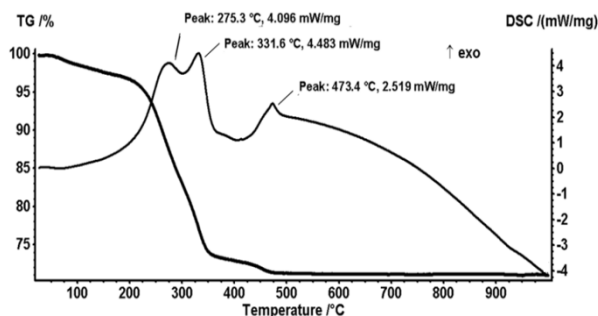


Fig. 4. TG-DSC analysis of $\text{Fe}_3\text{O}_4@\text{Zn-2}$

Both $\text{Fe}_3\text{O}_4@\text{Zn-1}$ and $\text{Fe}_3\text{O}_4@\text{Zn-2}$ nanoparticles exhibit on their TG-DSC curves one exothermic effect at ~ 449 °C/ ~ 473 °C attributed to the phase change of $\gamma\text{-Fe}_2\text{O}_3$ to $\alpha\text{-Fe}_2\text{O}_3$. $\gamma\text{-Fe}_2\text{O}_3$ is known as metastable intermediate in the oxidation of Fe_3O_4 [37].

3.2.3. High-resolution transmission electron microscopy (HRTEM)

The results of high-resolution transmission electron microscopy (Fig. 5 and 6) revealed that the as-prepared $\text{Fe}_3\text{O}_4@\text{Zn-1}$, and $\text{Fe}_3\text{O}_4@\text{Zn-2}$ nanoparticles were nearly spherical shape with narrow size distribution (average particle size of 3 nm for both compounds – Fig. 5b, Fig. 6b). HRTEM images (Fig. 5a and 6a) show that the nanoparticles are structurally uniform with lattice fringe spacing of 0.297 nm, 0.253 nm, 0.242 nm, 0.210 nm, which correspond to the (220), (311), (222), (400) lattice plane of the cubic Fe_3O_4 obtained from the JCPDS database (JCPDS card 75-1610).

Electron diffraction patterns for $\text{Fe}_3\text{O}_4@\text{Zn-1}$ (Fig. 5a-inset image) and $\text{Fe}_3\text{O}_4@\text{Zn-2}$ (Fig. 6a-inset image) showed that the samples are polycrystalline and they can be indexed to the spinel structure of Fe_3O_4 . The SAED patterns taken from a monolayer of $\text{Fe}_3\text{O}_4@\text{Zn-1}$ and $\text{Fe}_3\text{O}_4@\text{Zn-2}$ nanoparticles, contain 5, respectively 4, well-spotted rings. The corresponding interplanar spacings calculated from the SAED patterns are presented in Table 2.

Table 2. Interplanar spacings, $d(\text{\AA})$, deduced from SAED patterns analysis

	Diffraction ring, $d(\text{\AA})$				
	1	2	3	4	5
$\text{Fe}_3\text{O}_4@Zn-1$	2.97	2.53	2.09	1.62	1.48
$\text{Fe}_3\text{O}_4@Zn-2$	2.97	2.53	2.09	-	1.48
hkl	220	311	400	333	440

To confirm the binding of Zn-complexes on the surface of Fe_3O_4 nanoparticles, EDAX measurements were performed. The EDAX patterns of a) $\text{Fe}_3\text{O}_4@Zn-1$ and b) $\text{Fe}_3\text{O}_4@Zn-2$ revealed (without being quantitative), the presence of Fe, O and Zn elements. The peaks attributed to Cu were caused by copper grid (Fig. 7).

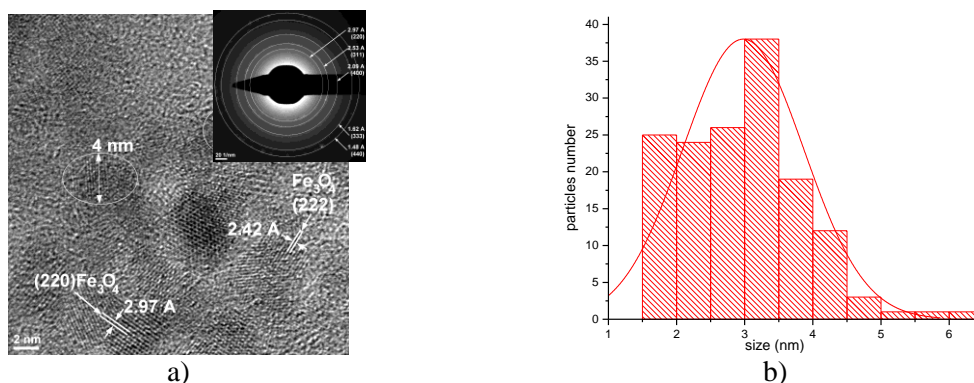


Fig. 5. a) HRTEM image of $\text{Fe}_3\text{O}_4@Zn-1$ – SAED image as inset graph b) particle size distribution of $\text{Fe}_3\text{O}_4@Zn-1$ (asymmetric unimodal distribution with the particles size distribution centered at 1.5-3.5 nm)

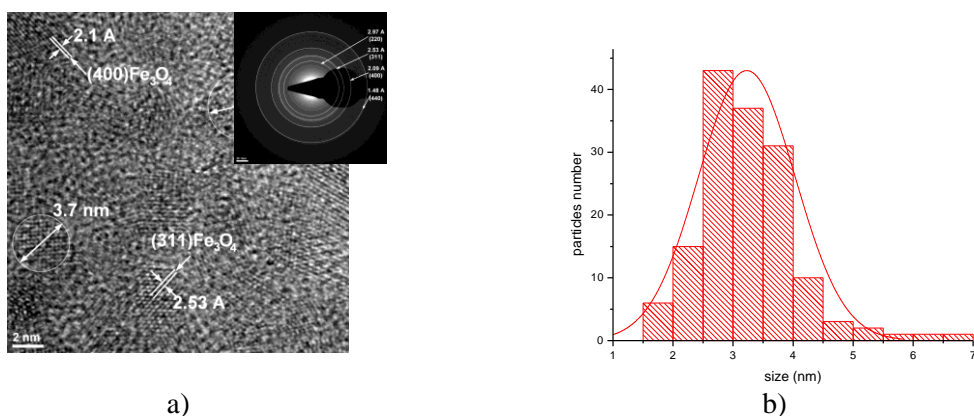


Fig. 6. a) HRTEM image of $\text{Fe}_3\text{O}_4@Zn-2$ – SAED image as inset graph b) particle size distribution of $\text{Fe}_3\text{O}_4@Zn-2$ (asymmetric unimodal distribution with the particles size distribution centered at 2.5-4 nm)

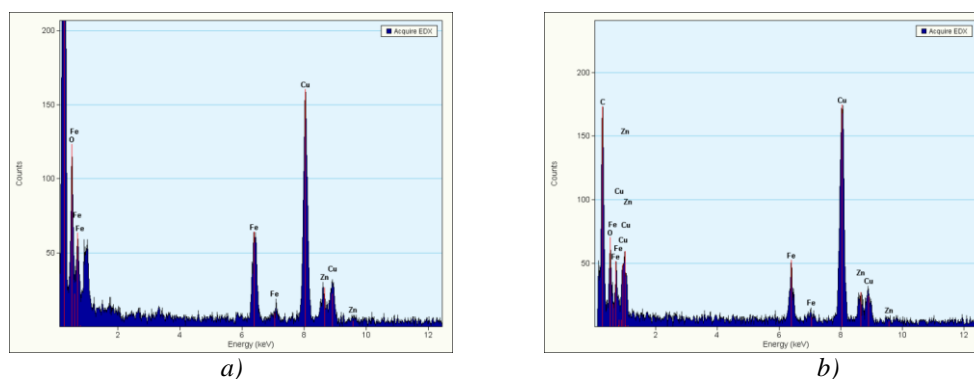


Fig. 7. EDAX patterns of a) $Fe_3O_4@Zn-1$ and b) $Fe_3O_4@Zn-2$

3.2.4. Preliminary biological assays

Preliminary results of flow cytometry examination of $Fe_3O_4@Zn-1$ showed that the nanoparticles induced no significant changes of cell cycle, both in HCT-8 and MSC cell lines, similar with untreated sample.

$Fe_3O_4@Zn-1$ nanoparticles are highly biocompatible both in HCT-8 and MSC cell line since the number of cells after incubation (24h, at 37 °C in 5% CO_2) with $Fe_3O_4@Zn-1$ nanoparticles was nearly equal to the number of cells in negative control group (Fig. 8).

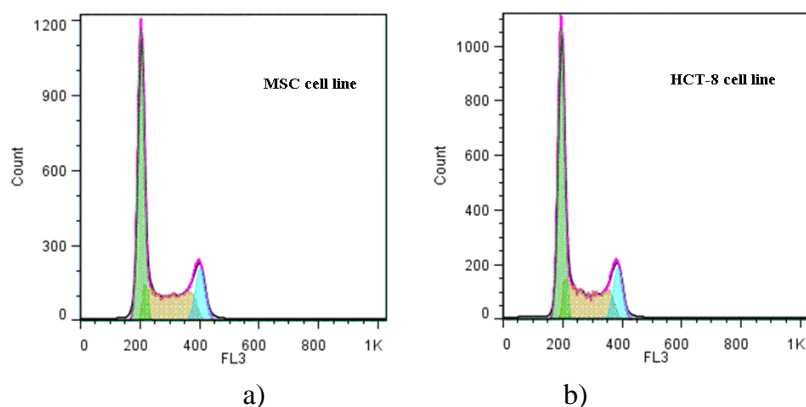
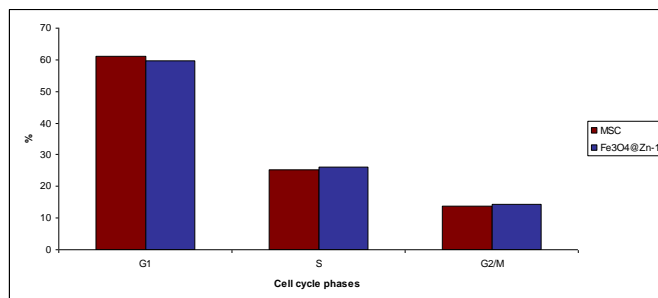


Fig. 8. Flow cytometry analysis diagrams on a) MSC cells and b) HCT-8 cells treated with $Fe_3O_4@Zn-1$ particles, at a final concentration of 1 mg/mL. The treatment was done for 24 h, at 37 °C and 5% CO_2 .

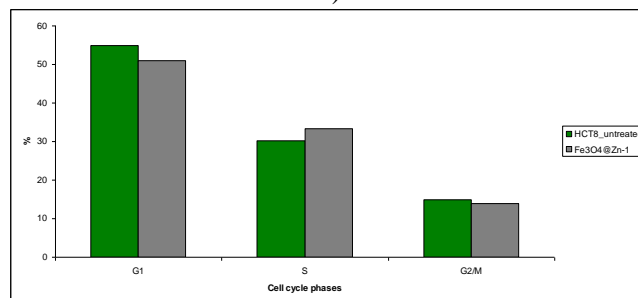
From flow cytometry analysis diagrams, it can be seen that no significant decrease has been obtained for G1, G2/M and S phases (Fig. 8, a and b).

The most intense changes were obtained for synthesized $Fe_3O_4@Zn-1$ powder, tested on HCT-8 cells, by inducing a significant decrease of the cells in G1 phase of the cell cycle, and slightly in S and G2/M phases (Fig. 9, a and b).

Cell cycle analysis showed no significant changes MSC cells upon treatment with synthesized $Fe_3O_4@Zn-1$ powders.



a)

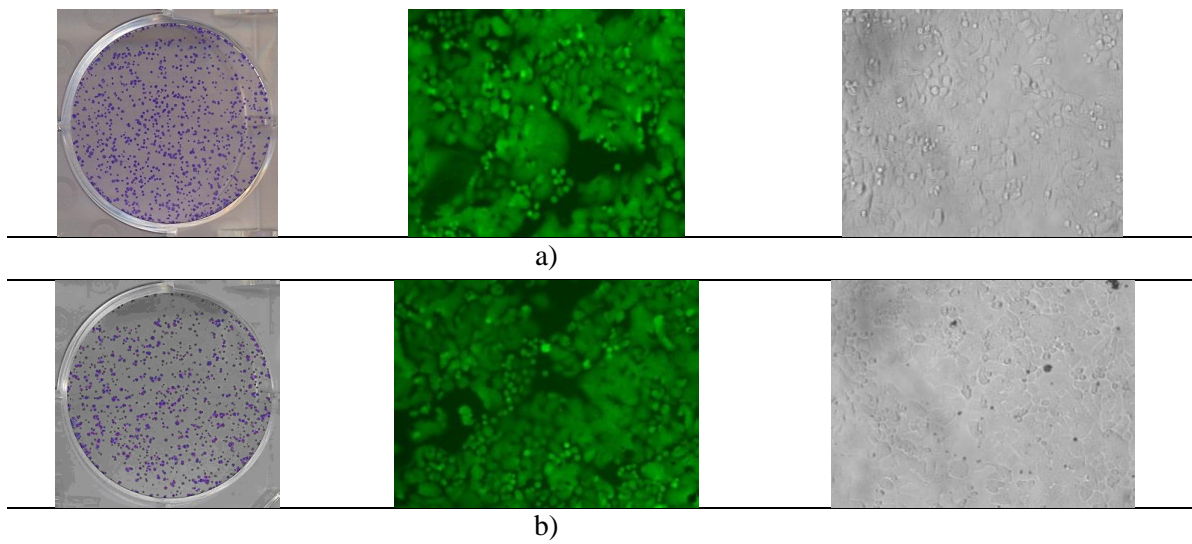


b)

Fig.9. Graphic representation of flow cytometry results
 a) MSC cell line treated for 24 h with synthesized Fe₃O₄@Zn-1 powders
 b) HCT-8 cell line, and at a final concentration of 1 mg/mL
 The treatment was done for 24 h, at 37 °C and 5% CO₂.

Cloning studies

The cloning experiment of Fe₃O₄@Zn-1 on HCT-8 cells has been investigated by treating cells for 24 h at 37 °C, 5% CO₂, with Fe₃O₄@Zn-1 synthesized powder. The results are presented in Fig. 10.



b)

Fig. 10. Cloning studies (left image -Invasion of HCT-8 cells in vitro; after 24h incubation, the invading cells were fixed with formaldehyde and stained with crystal violet), viability (middle image) and morphology (right image) of HCT-8 untreated cells, a), and HCT-8 cells treated with Fe₃O₄@Zn-1, b), at 37 °C, 5% CO₂

Cloning studies have underlined the obtaining of significant cellular clones, indicating that Fe₃O₄@Zn-1 powder induced high viability to HCT-8 cells. Thus the results showed that the obtained powder is biocompatible since it does not influence the viability of the eukaryotic cells.

4. Conclusions

Ultra-small pure phase-magnetite nanoparticles (average particle size of 3 nm for both Fe₃O₄@Zn-1 and Fe₃O₄@Zn-2) have been obtained *via* the polyol process starting from Fe(acac)₃ and PEG 200. Further surface functionalization with crystalline and well-characterized Zn(II)-carboxylato complexes (Zn-squarate and Zn-monomethyl terephthalate complexes) of these nanoparticles afforded the obtaining of bifunctional nanomaterials with magnetic core and coordinated Zn(II)-ions on the surface. XPS, TG-DSC and HRTEM/EDAX analyses were used to characterize the structure and the morphology of these new materials.

The developed method represents a green and facile route that can be used for scaled preparations. The proposed method contributes to the development of new catalysts, functional magnetic and optoelectronic materials, and biocompatible magnetic materials for their application in biology.

Preliminary biological assays on the Fe₃O₄@Zn-1 nanoparticles suggested that these bifunctional materials have low or none cytotoxicity on the tested biological targets.

Acknowledgements

The authors acknowledge financial support from the European Social Fund through POSDRU/89/1.5/S/54785 project: 'Postdoctoral Program for Advanced Research in the field of nanomaterials'.

References

- [1] J. H. Lee, Y. M. Huh, Y. Jun, J. Seo, J. Jang, H. T. Song, S. Kim, E. J. Cho, H. G. Yoon, J. S. Suh, J. Cheon, *Nat. Med.* **13**, 95 (2007).
- [2] J. Miyawaki, M. Yudasaka, H. Imai, H. Yorimitsu, H. Isobe, E. Nakamura, S. Iijima, *Adv. Mater.* **18**, 1010 (2006)
- [3] A. K. Gupta, M. Gupta, *Biomaterials* **26**, 3995 (2005)
- [4] S. Laurent, D. Forge, M. Port, A. Roch, C. Robic, L. Vander Elst, R.N. Muller, *Chem. Rev.* **108**, 2064 (2008).
- [5] W. Weiss, W. Ranke, *Prog. Surf. Sci.* **70**, 1 (2002)
- [6] M.K. Krause, M. Ziese, R. Hohne, A. Pan, A. Galkin, E. Zeldov, *J. Magn. Magn. Mater* **1097**, 242 (2002).
- [7] D. Beydoun, R. Amal, G.K.-C. Low, S. McEvoy, *J. Phys. Chem. B* **104**, 4387 (2000)
- [8] S. Mallakpour, M. Madani, *Prog. Org. Coat.* **86**, 194 (2015)
- [9] X. Cui., S. Belo, D. Krüger, Y. Yan, R. T. M. de Rosales, M. Jauregui-Osoro, H. Ye., S. Su, D. Mathe, N. Kovács, I. Horváth, M. Semjani, K. Sunassee, K. Szigeti, M. A. Green, P. J. Blower, *Biomaterials.* **35**, 5840 (2014)
- [10] C. J. Sunderland, M. Steiert, J. E. Talmadge, A. M. Derfus, S.E. Barry, *Drug Dev. Res.* **67**, 70 (2006)
- [11] A. Ito, M. Shinkai, H. Honda, T. Kobayashi, *J. Biosci. Bioeng.* **100**, 1 (2005).
- [12] H. Choi, S. R. Choi, R. Zhou, H. F. Kung, I.W. Chen, *Acad. Radiol.* **11**, 996 (2004).
- [13] S.P. Lin, J. Brown, *J. Magn. Reson. Imaging* **25**, 884 (2007).
- [14] S.V. Salihov, Y.A. Ivanenkov, S.P. Krechetov, M.S. Veselov, N.V. Sviridenkova, A.G., Savchenko, N.L. Klyachko, Y.I. Golovin, N.V. Chufarova, E.K. Beloglazkina, *J. Magn. Mater.* **394**, 173 (2015)
- [15] H. H. Yang, S. Q. Zhang, X. L. Chen, Z. X. Zhuang, J. G. Xu, X. R. Wang, *Anal. Chem.*

- 76**, 1316 (2004)
- [16] C. Boyer, M. R. Whittaker, V. Bulmus, J. Liu, T. P. Davis, *NPG Asia Mater.* **2**(1), 23 (2010).
- [17] I. Bilecka, I. Djerdj, M. Niederberger, *Chem. Commun.* 2008, 886-888.
- [18] S. H. Sun, H. Zeng, D. B. Robinson, S. Raoux, P. M. Rice, S. X. Wang, G. X. Li, *J. Am. Chem. Soc.* **126**, 273 (2004)
- [19] E. H. Kim, H. S. Lee, B. K. Kwak, B. K. Kim, *J. Magn. Magn. Mater.* **289**, 328 (2005)
- [20] W. Y. Teoh, R. Amala, L. Mädler, *Nanoscale* **2**, 1324 (2010)
- [21] H. Lee, M. K. Yu, S. Park, S. Moon, J. J. Min, Y. Y. Jeong, H.-W. Kang, S. Jon, *J. Am. Chem. Soc.* **129**, 12739 (2007)
- [22] Y. Sahoo, H. Pizem, T. Fried, D. Golodnitsky, L. Burstein, C. N. Sukenik, G. Markovich, *Langmuir* **17**, 7907 (2001)
- [23] L. Wang, Z. Yang, J. Gao, K. Xu, H. Gu, B. Zhang, X. Zhang, B. Xu, *J. Am. Chem. Soc.* **128**, , 13358 (2006).
- [24] A.-H. Lu, E. L. Salabas, F. Schüth, *Angew. Chem. Int. Ed.* **46**, 1222 (2007)
- [25] G. Gao, R. Shi, W. Qin, Y. Shi, G. Xu, G. Qiu, X. Liu, *J Mater Sci* **45**, , 3483 (2010)
- [26] J.-J. Lee, K. J. Jeong, M. Hashimoto, A. H. Kwon, A. Rwei, S. A. Shankarappa, J. H. Tsui, D. S. Kohane, *Nano Lett.*, **14**, 1 (2014)
- [27] W. Cai, J. Wan, *Journal of Colloid and Interface Science* **305**, 366 (2007)
- [28] Q. M. Kainz, A. Späth, S. Weiss, T. D. Michl, A. Schätz, W. J. Stark, B. König, O. Reiser, *Chemistry Open* **1**, 125 (2012)
- [29] D. Maity, S. N. Kale, R. Kaul-Ghanekar, J.-M. Xue, J. Ding, *J. Magn. Magn. Mater* **321**, , 3093 (2009)
- [30] M.-D. Şerb, B. Braun, O. Oprea, F. Dumitru, *Digest J. Nanomat. and Biostructures* **8**, 797 (2013)
- [31] M.-D. Şerb, Y. Wang, F. Dumitru, U. Englert, *Acta Cryst.* **E67**, m475 (2011)
- [32] U. I. Tromsdorf, O. T. Bruns, S. C. Salmen, U. Beisiegel, H. Weller, *Nano Lett.* **9**, 4434 (2009)
- [33] J.-J. Lee, K. J. Jeong, M. Hashimoto, A. H. Kwon, A. Rwei, S. A. Shankarappa, J. H. Tsui, D. S. Kohane, *Nano Lett.*, **14**(1), 1 (2014)
- [34] A. P. Grosvenor, B. A. Kobe, M. C. Biesinger, N. S. McIntyre, *Surf. Interface Anal.*, **36**, 1564 (2004)
- [35] X. Teng, D. Black, N. J. Watkins, Y. Gao, H. Yang, *Nano Lett.* **3**(2), 261 (2003)
- [36] Z. Mekhalif, L. Massi, F. Guittard, S. Geribaldi, J. Delhalle, *Thin Solid Films* **405**, 186 (2002)
- [37] J. P. Sanders, P. K. Gallagher, *Thermochim. Acta* **406**, 241 (2003)